Supporting Information

A cathode-supported-electrolyte configuration for high performance all solid-state lithium-sulfur batteries

Liu Wang[1, +], Xuesong Yin[2, +], Chengbin Jin[1, 3], Chen Lai[1, 4], Gan Qu[1, 5], Guangyuan Wesley Zheng[1,2]*

[1] Department of Chemical and Biomolecular Engineering, National University of Singapore, 117585 Singapore.

[2] Institute of Materials Research and Engineering, A*STAR (Agency for Science, Technology and Research), 138634 Singapore.

[3] College of Materials Science and Engineering, Zhejiang University of Technology, Hangzhou 310014, China.

[4] School of Chemical Engineering and Technology, Xi'an Jiaotong University, Xi'an 710049, China.

[5] College of Materials Science and Engineering, Zhengzhou University, Zhengzhou 450001, China.

[+] Equal contributors

*Corresponding author. E-mail: chezg@nus.edu.sg, wesley-zheng@imre.a-star.edu.sg

Experimental Methods

Solid polymer electrolyte slurry and free-standing electrolyte membrane preparation

Powder mixture with an appropriate ratio of PEO (MW=100k), PVDF, LiTFSI and BN were dispersed in 1-Methyl-2-pyrrolidone under vigorous magnetic stirring at 100 ^{o}C for 12 h, resulting a viscous white slurry with a high concentration of 0.25 g/mL (PEO+PVDF+LiTFSI+BN in NMP). The free-standing solid polymer electrolyte membrane was fabricated by blade casting the as-prepared slurry on Al foil followed by solvent evaporation at 80 ^{o}C for 24 h. Then the free-standing

membrane with a thickness of 20~30 μm can be peeled off from the substrate. The proportion of PEO, PVDF, LiTFSI and BN in the polymer electrolyte is 3:1:1:1 in this work.

Fabrication of sulfur cathode and cathode-supported-electrolyte bilayer

PEO-LiTFSI slurry was prepared by dissolving PEO of different MW (4000k and 600k) and LiTFSI with a [EO]/Li ratio of 20 in 1-Methyl-2-pyrrolidone. The resulting transparent gel was served as ionic conductive component and binder. S/C composite powder was obtained by ball-milling sublimed sulfur powder and super P with a mass ratio of 8:3 for 20 h. Then S/C composite and additional super P was dispersed in the PEO-LiTFSI slurry under magnetic stirring, leading to a homogeneous slurry for electrode fabrication. The S/C composite electrode was obtained by blade casting the abovementioned slurry on Al foil followed by drying at 60 ^{o}C for 20 h. The as-prepared cathode consists 40% sulfur, 30% conductive carbon and 30% PEO-LiTFSI with a sulfur mass loading of ~0.6 mg/cm^2. The cathode-supported-electrolyte bilayer was fabricated by directly casting the electrolyte slurry on the cathode surface followed by drying at 80 ^{o}C for 24 h, delivering a homogeneous electrolyte layer and intimate cathode/electrolyte interface. Dry PEO-LiTFSI membranes with different MW were also made by casting and drying the ionic conductive binder for characterization.

Battery assembly

All solid-state Li-S batteries were assembled in Ar-filled glovebox without adding any liquid electrolyte. C-S-E/4000k and C-S-E/600k ASSLSBs were assembled by simply stacking Li foil on the electrolyte side of the cathode-supported-electrolyte bilayer in CR2032 coin cell cases. The laminated/4000k all solid-state Li-S battery was made by orderly laminating the free-standing electrolyte membrane and Li foil on the cathode. The bipolar all solid-state Li-S battery was

fabricated by connecting two mono full cells (cathode-supported-electrolyte bilayer | Li) in series. Free-standing cathode-supported-electrolyte bilayer was also applied as current collector-free cathode and electrolyte and combined with Li foil to construct all solid-state Li-S battery in coin cell case. All solid-state Li-S pouch cell was assembled by sealing cathode-supported-electrolyte bilayer | Li in Al-plastic film and applying nickel ribbons as tabs.

Materials characterizations

The surface and cross-section morphologies of the cathode, electrolyte and cathode/electrolyte interface were inspected by a field-emission scanning electron microscopy (FESEM) (JEOL, JSM 7600F). The elemental mapping was measured by energy dispersive X-ray spectroscopy (EDX). The crystalline structure was determined by X-ray diffraction (Bruker D8 Advance). Phase transition behaviour of the dry PEO-LiTFSI membrane was measured by differential scanning calorimetry (DSC 8000-Perkin Elmer) ranging from -80 to 100 ^{o}C with a heating rate of 10 ^{o}C/min. Mechanical properties were characterized by nano indentation system (MTS Nano Indenters® XP, TN, USA).

Electrochemical characterizations

Ionic conductivity was measured by electrochemical impedance spectroscopy (EIS) on electrochemical workstation (Biologic SP-300) under a sine wave with amplitude of 10 mV over a frequency range of 10 Hz to 3 MHz. The measured electrolyte was sandwiched between two stainless-steel blocking electrodes for testing. The electrochemical stability window of the free-standing electrolyte is determined by linear sweep voltammograms (LSV) with the incorporation of stainless steel (SS) as work electrode and Li foil as both counter and reference electrode. The LSV measurement was conducted between OCV (open-circuit voltage) and 6.0 V versus Li^{+}/Li

with a sweep rate of 1 mV/s. The battery performance was tested on Neware battery test system with a voltage range of 1.7-2.8 V at 0.1 C, and 1.5-2.8 V at higher C-rates (0.2-1.0 C), respectively. The bipolar all solid-state Li-S battery was operated on Arbin battery test system within 3.4-5.6 V.

Calculations

1. Contributions of each component to elemental signals in Figure 2b, c

In composite cathode in Figure 2b:

$S_{(LiTFSI)}$ = 64/287×7.5 wt% = 1.67 wt%;

$S_{(active\ material)}$ = 40 wt%;

$C_{(LiTFSI)}$ = 24/287×7.5 wt% = 0.63 wt%;

$C_{(carbon\ additive)}$ = 30 wt%.

So the sulfur and carbon signals are mostly originated from the active materials and conductive agents, respectively.

In polymer electrolyte in Figure 2c:

$N_{(LiTFSI)}$ = 14/287×16.7 wt% = 0.81 wt%;

$N_{(BN)}$ = 11/25×16.7 wt% = 7.35 wt%.

The nitrogen signal is mainly originated from BN rather than LiTFSI.

2. Energy densities with and without aluminum current collector

Energy densities were calculated according to the equation below:[1]

$E_g = V \times m_A \times C / \sum W_i$

in which

E_g=gravimetric energy density (Wh/kg);

V=average cell operating voltage (V, 2.0 here);

m_A=active material loading (mg/cm^2, 0.6 here);

C=active material capacity (mAh/g, 1034 for battery with current collector and 900 for free-standing one);

W_i=areal density of individual components (g/cm^2).

The areal densities of individual cell components are listed in the following table (the packing weight is excluded for calculation).

Table S1. Areal densities of individual components and total cell with or without current collector. (unit: mg/cm^2)

Cathode	Electrolyte	Lithium (100 μm)	Current collector	$\sum W_i$ (free-standing)	$\sum W_i$ (with current collector)
1.5	2.9	5.3	4.3	9.7	14.0

$E_{g(\text{free-standing})} = 2\times0.6\times900/9.7=111.4$ Wh/kg;

$E_{g(\text{with current collector})} = 2\times0.6\times1034/14.0=88.6$ Wh/kg.

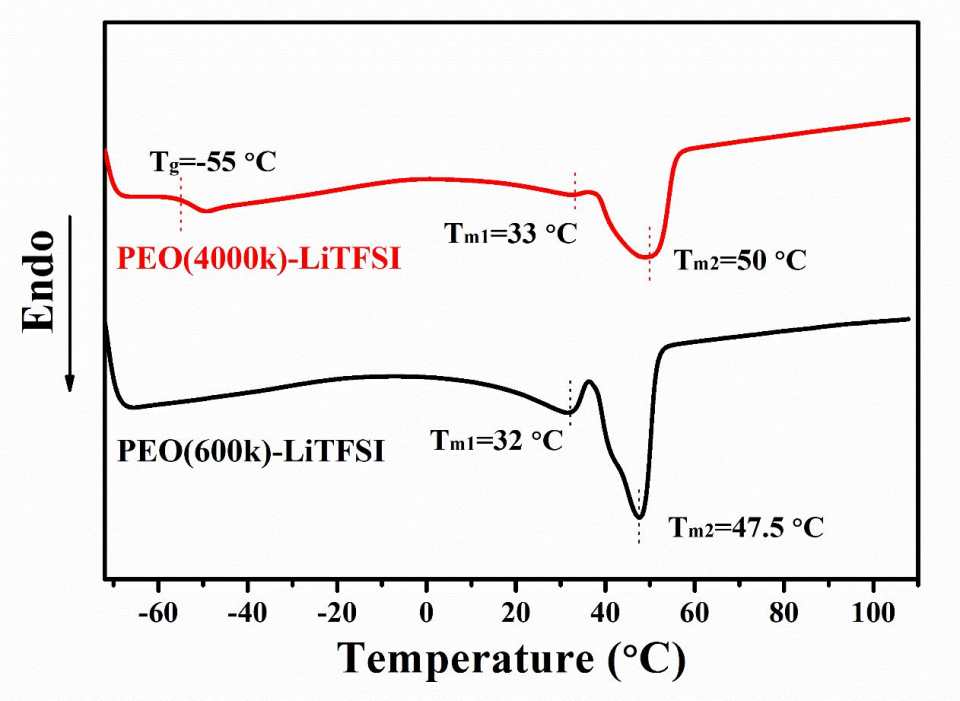

Figure S1. Differential scanning calorimeter (DSC) curves of PEO(4000k)-LiTFSI and PEO(600k)-LiTFSI. PEO(4000k)-LiTFSI presents a higher melting point of 50 ^{o}C (T_{m2}) for crystalline PEO and an unobvious melting of eutectic mixture of PEO and LiTFSI at 33 ^{o}C (T_{m1}). Whereas PEO(600k)-LiTFSI shows a distinct melting behavior at a relatively low temperature of 32 ^{o}C (T_{m1}), and its melting point of crystalline PEO (47.5 ^{o}C) is also lower than that of PEO(4000k)-LiTFSI.

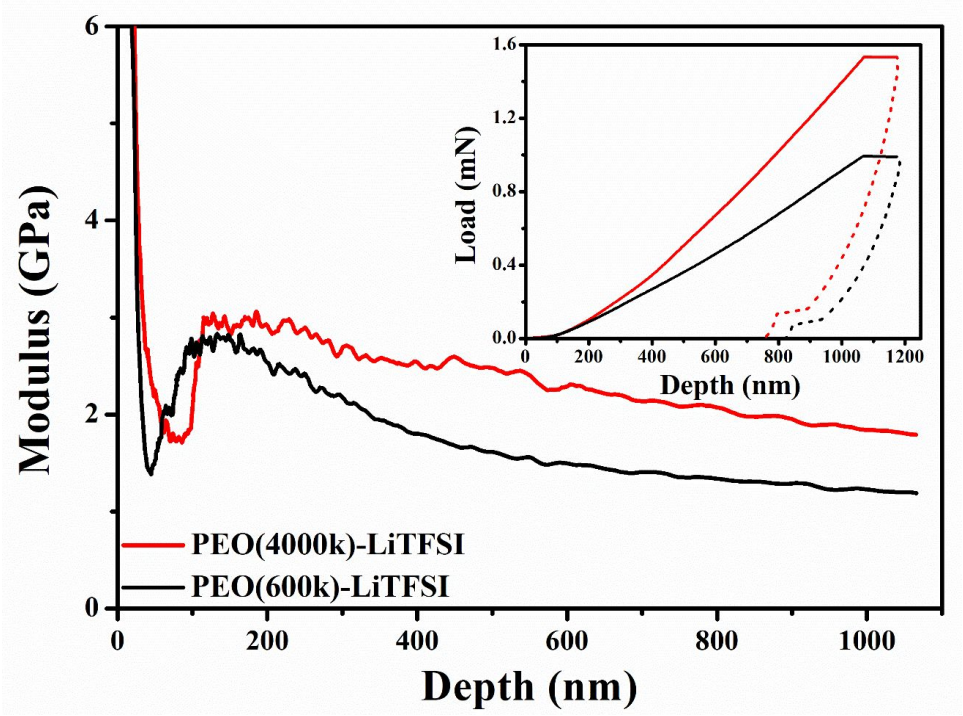

Figure S2. Nanoindentation profiles of PEO(4000k)-LiTFSI and PEO(600k)-LiTFSI. The elastic modulus of PEO(4000k)-LiTFSI outperforms that of PEO(600k)-LiTFSI, demonstrating its beneficial mechanical performance as a strong binder.

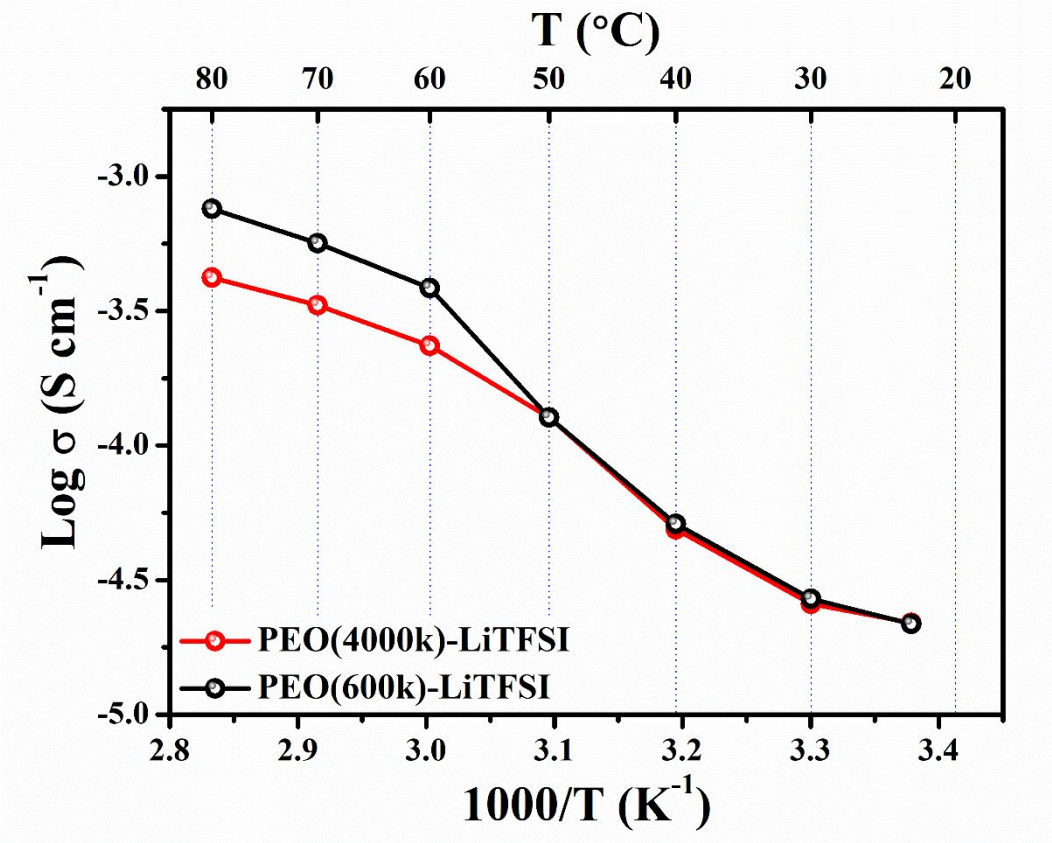

Figure S3. Arrhenius ionic conductivity plots of PEO(4000k)-LiTFSI and PEO(600k)-LiTFSI. At room temperature to 50 °C, the ionic conductivity of PEO(4000k)-LiTFSI is comparable to that of PEO(600k)-LiTFSI; and at 60~80 °C, it is only slightly lower than the latter one. Even so, the ionic conductivity of either binder is high enough for battery operation (>10^{-4} S cm^{-1}) at temperature higher than 50 °C.

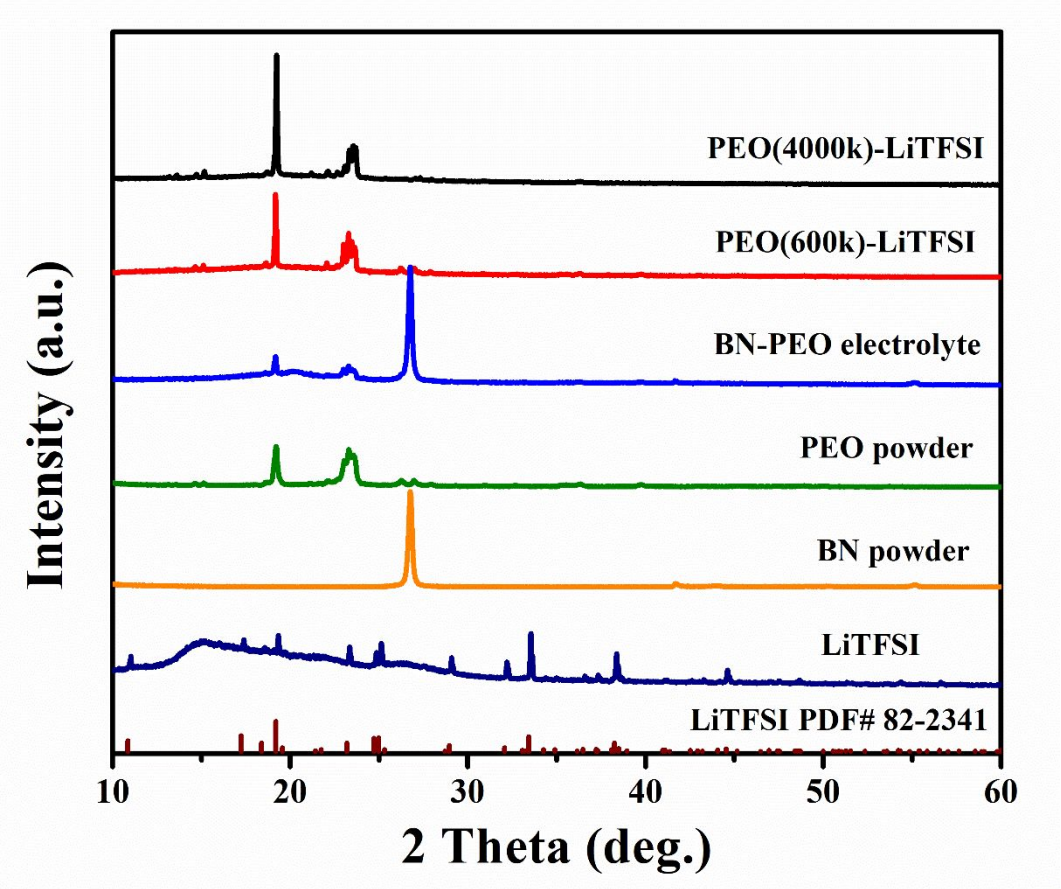

Figure S4. XRD pattens of BN-PEO electrolyte, PEO(4000k)-LiTFSI and PEO(600k)-LiTFSI binders, as well as the raw materials of BN, LiTFSI and PEO powder.

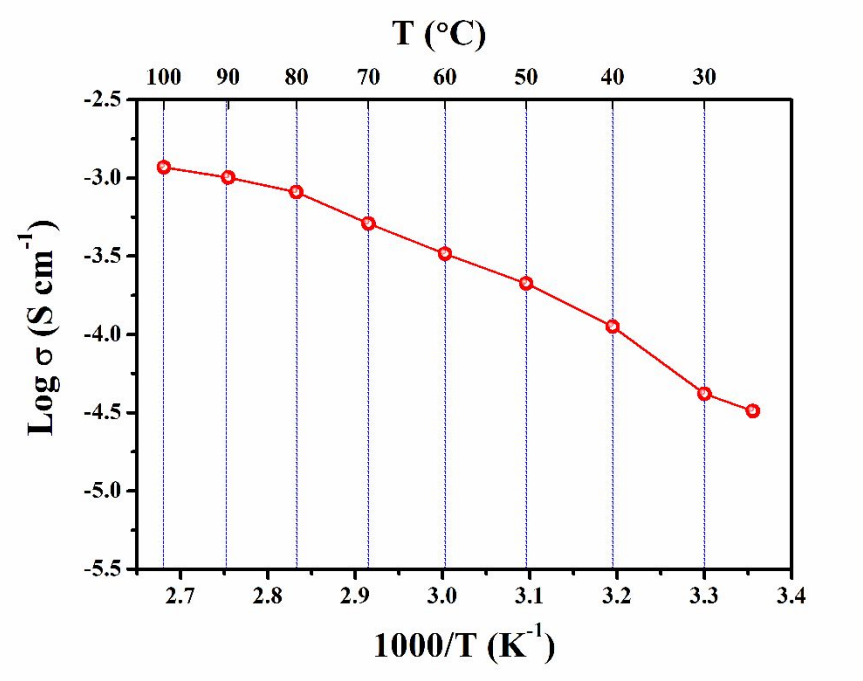

Figure S5. Arrhenius ionic conductivity plots of BN-PEO electrolyte.

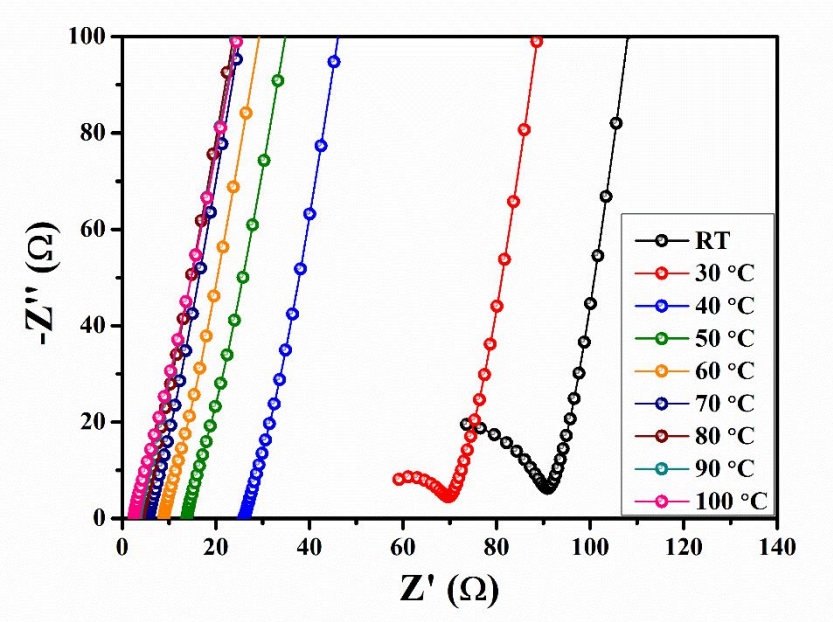

Figure S6. Nyquist plots of free-standing BN-PEO electrolyte with thickness of 30 μm at different temperatures.

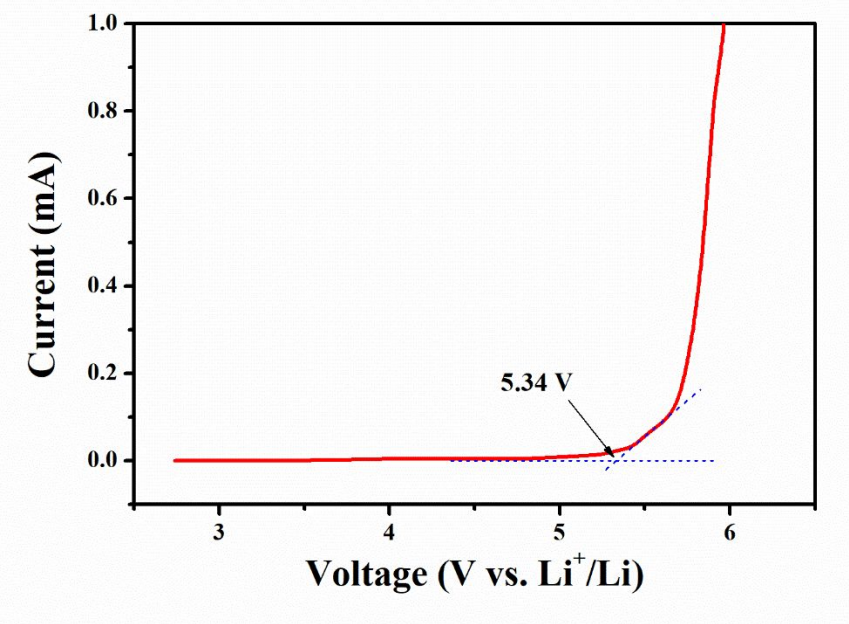

Figure S7. Electrochemical stability window evaluation of free-standing BN-PEO electrolyte with a structure of SS | BN-PEO electrolyte | Li at 55 ^{o}C. The sweep rate is 1 mV/s.

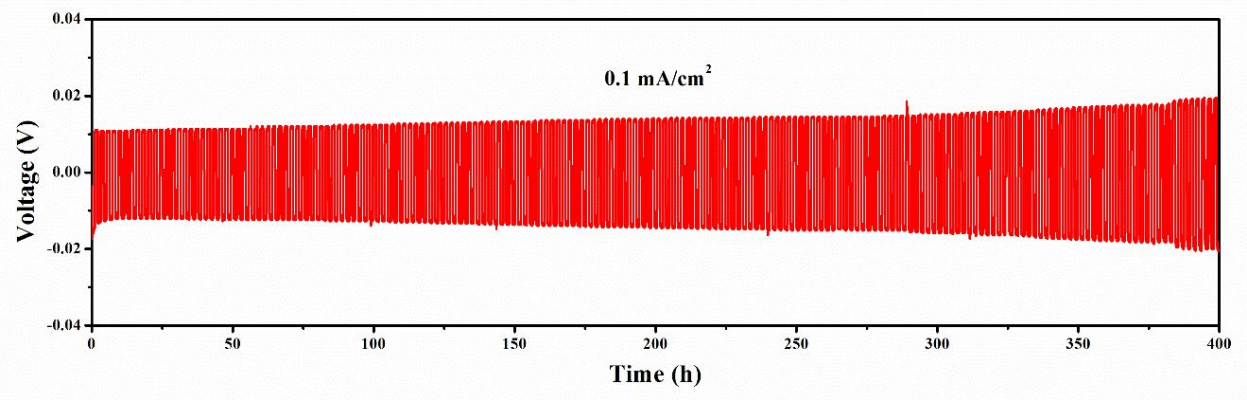

Figure S8. Long-term cycling of Li/Li symmetric cells with free-standing BN-PEO electrolyte at 55 °C at 0.1 mA/cm^2 with capacity of 0.1 mAh/cm^2. The overpotential gradually increases from 11 mV to 19 mV for 400 h without short circuit.

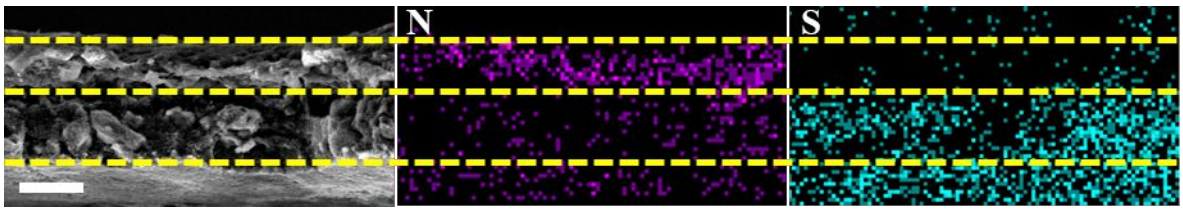

Figure S9. Cross-section SEM image of the cathode-supported-electrolyte bilayer and the corresponding elemental mapping of nitrogen and sulfur. Scale bar: 20 μm.

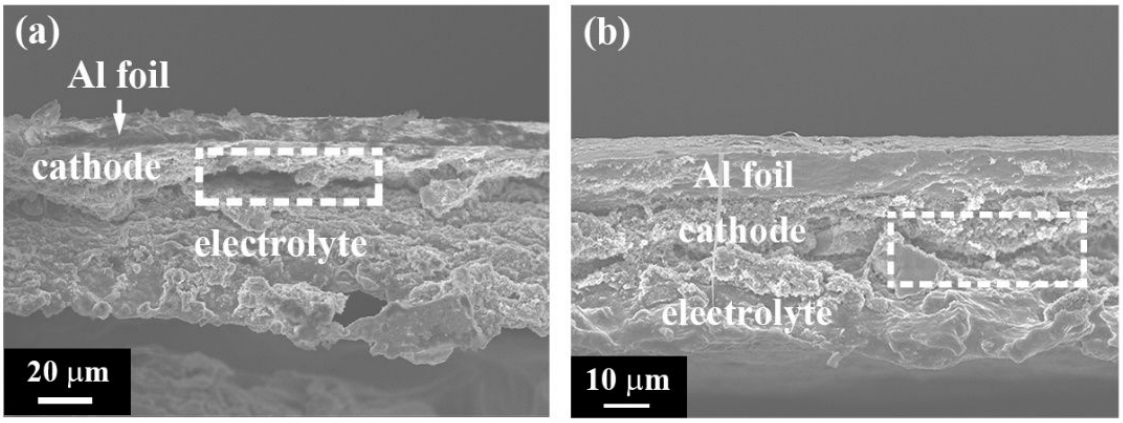

Figure S10. Cross-section SEM images of the laminated cathode-electrolyte bilayer with loose contact (a) and gaps (b) at the interface as shown in the white dashed rectangles.

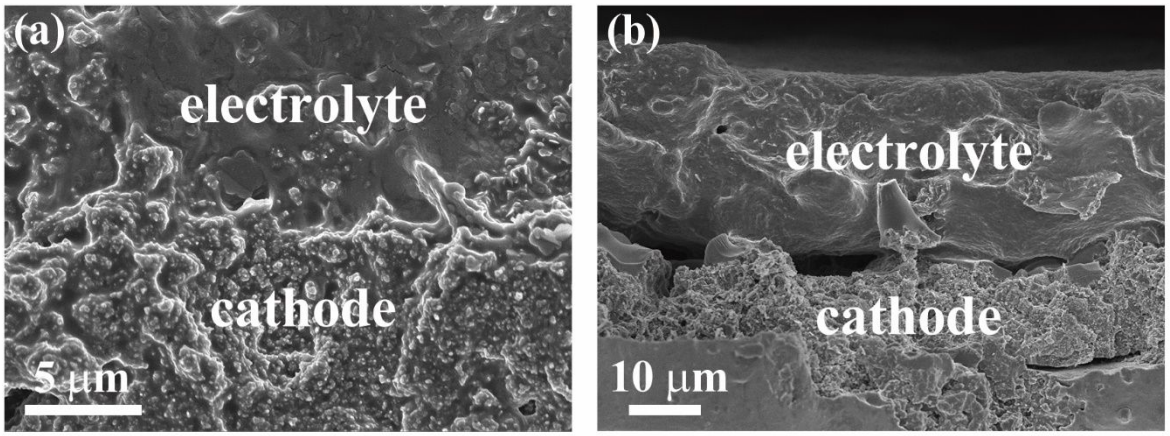

Figure S11. Electrolyte-cathode cross-sections of the cathode-supported-electrolyte structure (a) and the laminated structure (b) after heating at battery operation temperature (55 ^{o}C) for 24h.

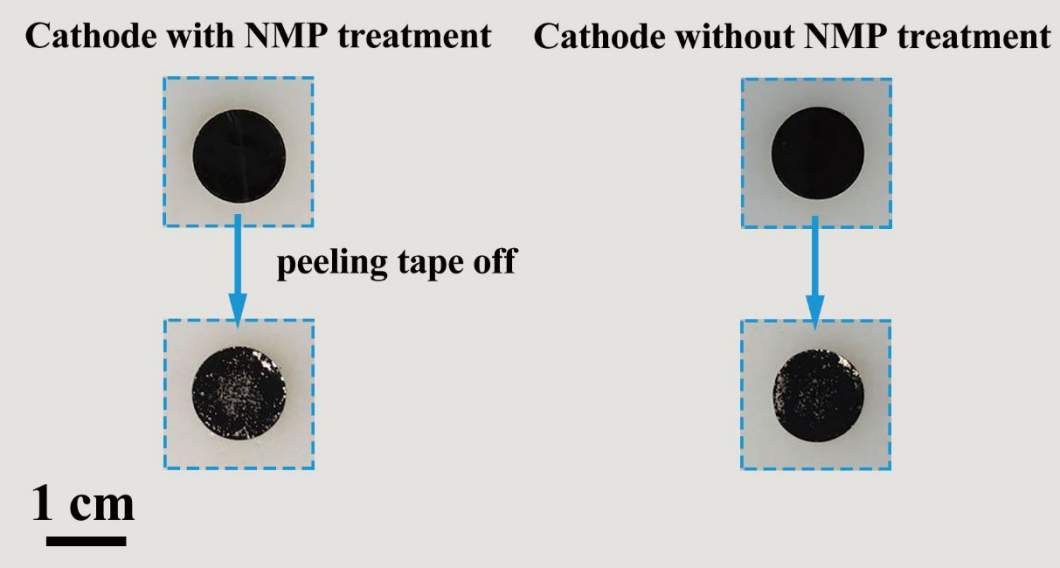

Figure S12. Tape test of cathode with (left) and without (right) NMP treatment. 20 μL NMP was dropped on one cathode plate. Then the cathode was heated at 80 ^{o}C for 24 h, consistent with the casted electrolyte drying condition. A piece of tape was pasted on the cathode and then peeled off.

Figure S13. Digital image of a free-standing cathode-supported-electrolyte bilayer.

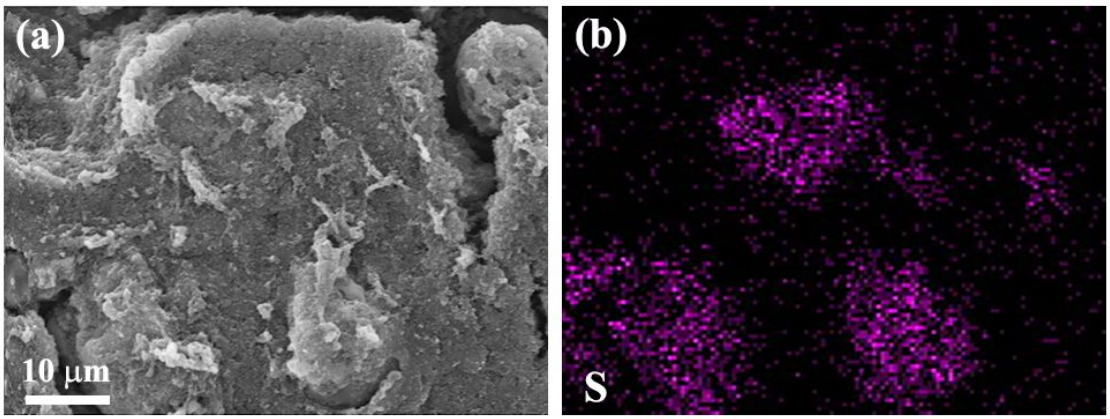

Figure S14. (a) SEM image and (b) sulfur mapping of the post-mortem cathode surface with PEO(600k)-LiTFSI.

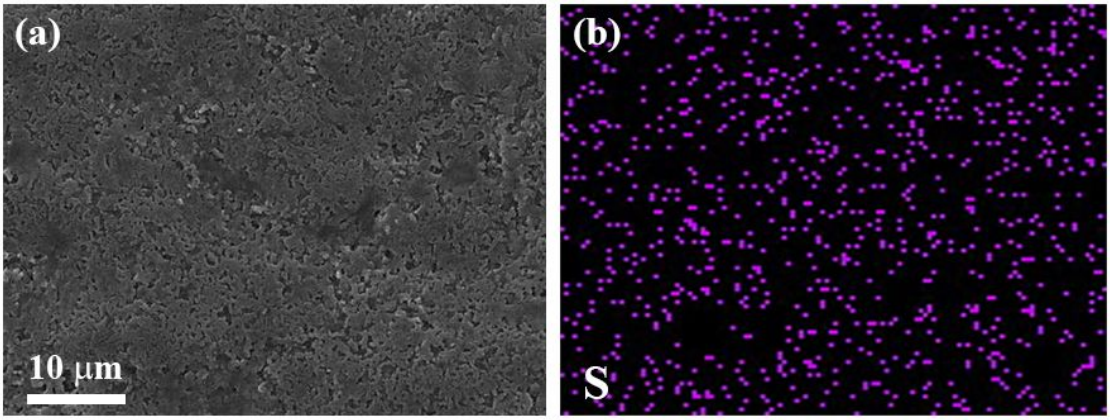

Figure S15. (a) SEM image and (b) sulfur mapping of the post-mortem cathode surface with PEO(4000k)-LiTFSI.

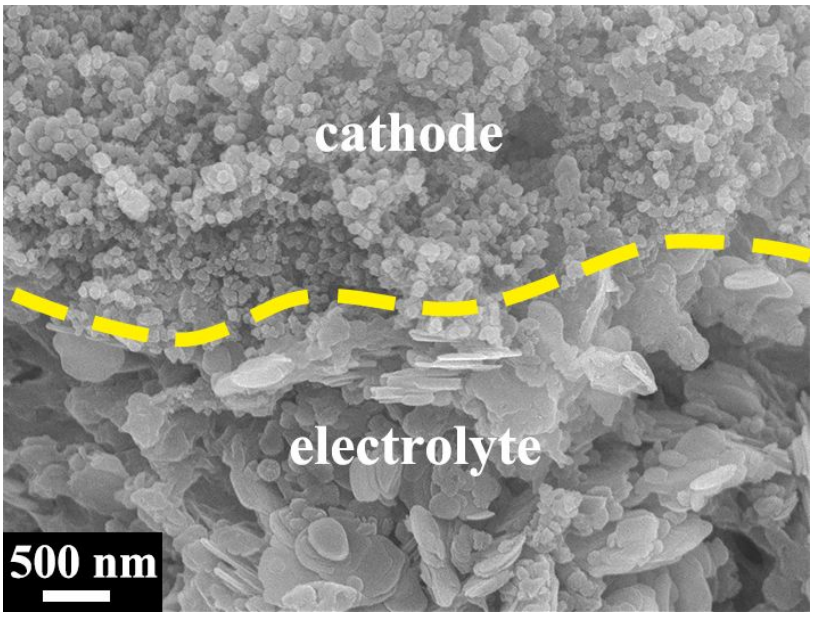

Figure S16. Cross-section SEM image of the post-mortem interface of the cathode-supported-electrolyte configuration.

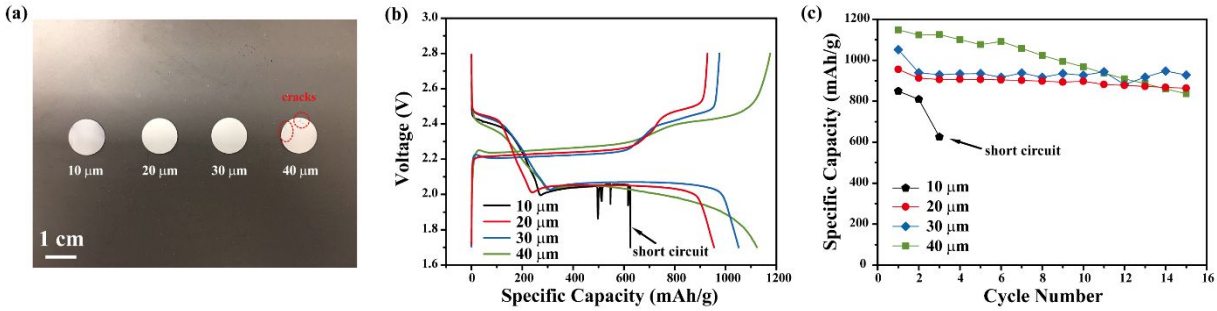

Figure 17. (a) Digital image of cathode-supported-electrolyte configurations with different electrolyte thickness ranging from 10 to 40 μm. (b) Charge-discharge profiles and (c) specific capacities of cells with different electrolyte thickness.

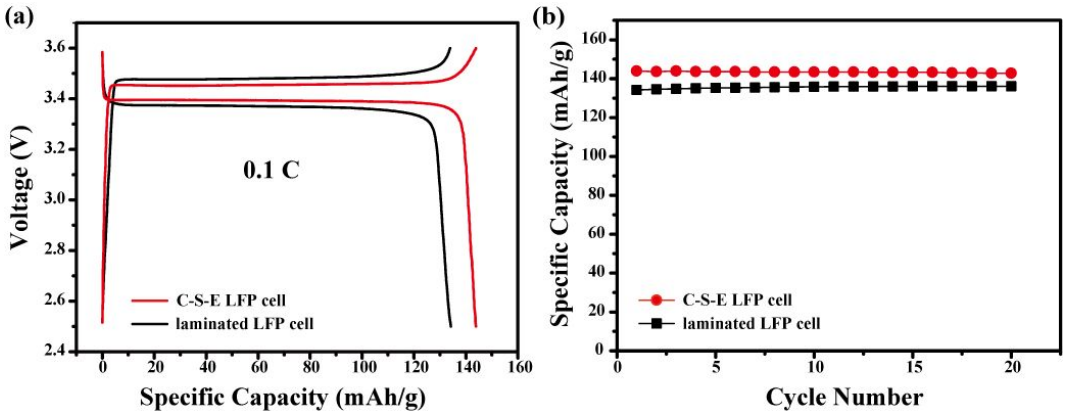

Figure 18. (a) Charge-discharge curves and (b) discharge capacities of Li-$LiFePO_4$ cell with different cathode-electrolyte structures at 0.1 C.

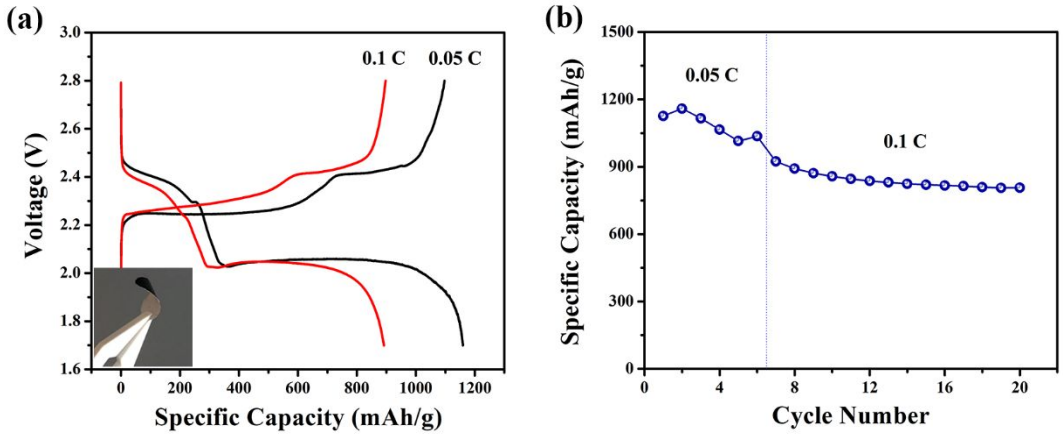

Figure S19. (a) Charge-discharge profiles of free-standing cathode-supported-electrolyte bilayer at 0.05, 0.1 C, and (b) the cycle performance.

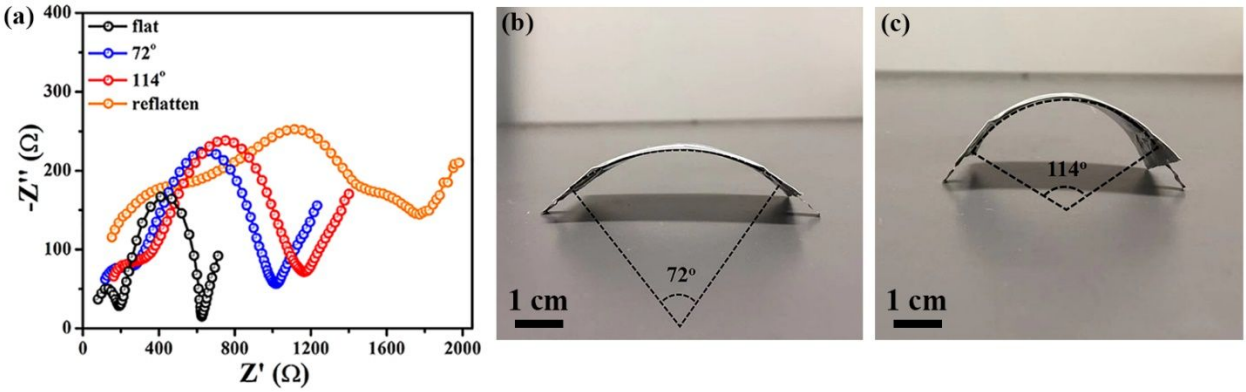

Figure S20. (a) EIS of pouch cell with laminated/4000k under different bending states. (b, c) Digital images of the laminated/4000k pouch cell under different bending levels.

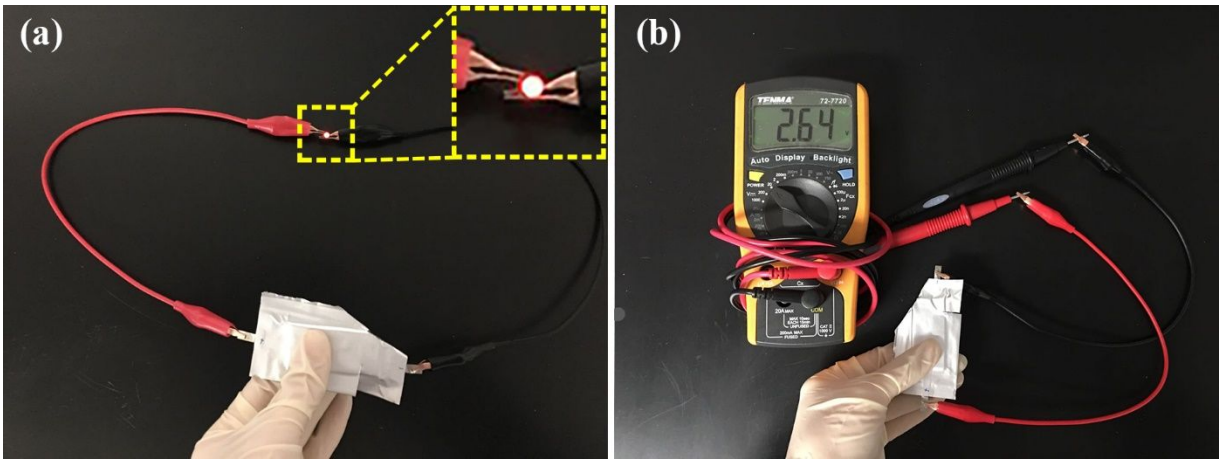

Figure S21. Cutting tests of the all solid-state Li-S pouch cell, which can (a) light a red LED and (b) show OCV of 2.64 V even suffering two scissor cuts.

Reference:

(1) McCloskey, B. D. Attainable Gravimetric and Volumetric Energy Density of Li–S and Li Ion Battery Cells with Solid Separator-Protected Li Metal Anodes. *The Journal of Physical Chemistry Letters* **2015,** *6,* 4581-4588.